Engineered Piezoelectricity in Graphene

Mitchell T. Ong and Evan J. Reed*

Department of Materials Science and Engineering, Stanford University, Stanford, California 94305, United States

ABSTRACT

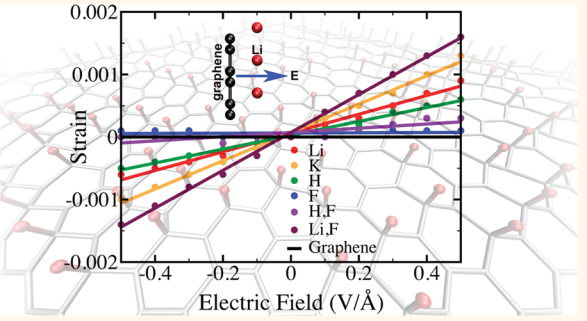

We discover that piezoelectric effects can be engineered into nonpiezoelectric graphene through the selective surface adsorption of atoms. Our calculations show that doping a single sheet of graphene with atoms on one side results in the generation of piezoelectricity by breaking inversion symmetry. Despite their 2D nature, piezoelectric magnitudes are found to be comparable to those in 3D piezoelectric materials. Our results elucidate a designer piezoelectric phenomenon, unique to the nanoscale, that has potential to bring dynamical control to nanoscale electromechanical devices.

KEYWORDS: graphene · piezoelectricity · adsorption · two-dimensional materials · density functional theory · nanoelectromechanical systems (NEMS)

Advances in nanoscale fabrication are leading to remarkably innovative devices for electronics, photonics, energy harvesting, and other applications.[1−4] Microelectromechanical systems (MEMS) are being extended to the nanoscale (NEMS)[5] in the context of nanosized actuators,[6,7] motors,[8] robots,[9] and locomotive devices.[10] The engineering of strain in the 2D material graphene[11] may provide avenues to novel 2D electronic devices.[12−19] A fundamental challenge with these technologies is being able to dynamically control motion and deformation at the nanoscale. Piezoelectric materials are frequently used for dynamical control of material deformation by the application of an external electric field and are central to a wide variety of applications from pressure sensors[20] to acoustic transducers[21] to high voltage generators.[2] Unfortunately, nanocarbon materials like 2D graphene are not intrinsically piezoelectric and are therefore not amenable to control with moderate electric fields. One would like to make graphene piezoelectric to endow dynamic control on existing graphene-based electronics and other devices. Piezoelectricity is traditionally thought to be an intrinsic property of a particular material phase, for example, wurtzite structure. On the contrary, here we find that piezoelectricity can be engineered into intrinsically nonpiezoelectric graphene. This new phenomenon is nanoscale, lacking a direct bulk analogue,[22,23] and provides practical paths toward manipulation and dynamic control of the optical, chemical, electronic, and other properties of nanoscale devices.

Graphene is a one-atom thick layer of carbon atoms arranged in a honeycomb lattice. This 2D carbon material has a number of anomalous optical and electronic properties, including extraordinarily high carrier mobility and being a zero band gap semimetallic conductor where the valence and conduction bands intersect at a single Dirac point. It is extremely mechanically flexible and one of the strongest known materials.[24] Graphene's realized applications include field-effect transistors (FETs)[3] and membranes that can be used to trap gases.[4] Recent experimental work has shown that it is possible to modify bilayer graphene's electronic properties by applying an electric field normal to the plane.[1] Further experimental control over electronic properties has been demonstrated in strained graphene,[25−27] where strain is found to have an effect similar to the application of a strong magnetic field.[12] Numerous theoretical efforts predict that the control and engineering of strain could lead to devices where electronic and optical properties can be manipulated using strategic mechanical deformations, dubbed straintronics.[14−18,28] Strain can be measured using a variety of experimental approaches,[26,29,30] and some of the first steps toward *dynamical,* reversible control of strain and ripples in graphene have been demonstrated utilizing temperature changes coupled to graphene's thermal expansion properties.[13]

* Address correspondence to evanreed@stanford.edu.

Received for review October 31, 2011 and accepted December 23, 2011.

Published online December 23, 2011
10.1021/nn204198g

In this work, we demonstrate that piezoelectricity can be engineered into graphene by chemical doping. A key characteristic of piezoelectric materials is that they belong to a noncentrosymmetric point group (*i.e.*, material without an inversion center).[31] Unlike its boron nitride counterpart, 2D h-BN,[32−34] graphene exhibits inversion symmetry, and thus, is not intrinsically piezoelectric. This inversion symmetry element must be broken in order to induce piezoelectricity. This can be accomplished by the adsorption of atoms on the surface of graphene only on one side. Unlike the case of 2D h-BN, the patterned adsorption of atoms allows one to selectively control the spatial regions on the sheet that are endowed with piezoelectricity. The one-sided doping of graphene and spatial control of adatom distribution required to achieve the structures considered in this work have been demonstrated in recent experiments.[35−39]

Chemical doping of graphene with adatoms is an active research area for both experiments[40,41] and theory.[42−45] Hydrogen and fluorine covered graphene (graphane and fluoro-graphene) have both been realized in the laboratory and are found to be chemically stable at ambient conditions.[35−37] Both of these materials have been synthesized in a form with adatom coverage on only one side of graphene, among the cases considered in this work. Surface structure and island formation of alkali metal atoms have also been studied on graphene and graphite.[41,46−50] We use density functional theory (DFT) to calculate the stress and strain piezoelectric coefficients for a variety of experimentally realizable adatoms on graphene and compare them to other piezoelectric materials. Furthermore, we examine how the piezoelectric coefficients vary as a function of adatom surface coverage.

RESULTS AND DISCUSSION

Our piezoelectric coefficient calculations are performed using DFT implemented within the Quantum-ESPRESSO *ab initio* software package[51] where exchange and correlation effects are described using the spin-polarized generalized−gradient corrected Perdew-Burke-Ernzerhof (PBE) approximation.[52] We have examined cases where graphene is doped with a uniform coverage of lithium (Li), potassium (K), hydrogen (H), and fluorine (F) atoms. We have also considered two different atom dopants on opposite sides, such as H and F, or F and Li. The unit cell and position of the adatoms used in this work are shown in Figure 1. For all cases, we employ periodic boundary conditions such that each adatom is associated with two carbon atoms. Our DFT calculations show that both Li and K prefer to bind to graphene at the hollow site, which is the center of the honeycomb, giving these structures hexagonal (6*mm*) point group symmetry. On the basis of the top site (directly over a carbon atom) bonding of covalent interactions,[36,53] we take H and F to bind at the top site resulting in trigonal (3*m*) symmetry. For the cases involving two atoms, both result in trigonal (3*m*) symmetry due to at least one of the two atoms binding at the top site. The point group symmetries for each of the six configurations mentioned above are summarized in Figure 2b. These are compared to point group symmetries for pure graphene (6/*mmm*) and hexagonal boron nitride (32) in Figure 2a. Of these, the 6*mm*, 32 and 3*m* point groups are noncentrosymmetric and therefore piezoelectric.

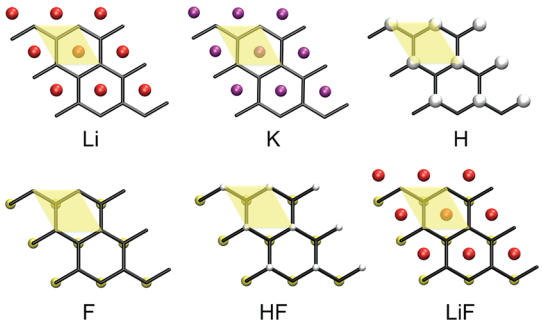

Figure 1. Unit cells for each of the adatom cases studied are highlighted in yellow. Periodic boundary conditions are employed in all cases.

From the point group symmetry, we can determine which piezoelectric coefficients are nonzero (see Supporting Information).[31] In this work, we focus on calculating the d_{31} and e_{31} coefficients, which are predicted by symmetry to be nonzero and are common to all six configurations depicted in Figure 2b. These coefficients relate in-plane strain to electric field and electrical polarization normal to the plane, and are relevant for the gate voltage geometries utilized in FETs.

Figure 3a shows how equibiaxial in-plane strain (*i.e.*, equal strain in the 1- and 2-directions) of graphene varies as a function of electric field applied perpendicular to the surface for the configurations in Figure 2b. This applied field was modeled using a periodic sawtooth potential[54] where the width of the saw was 10 Å. Comparing to pure graphene, we see that doping with atoms changes the electromechanical properties. We find that there is an approximately linear relationship between the field and strain at field amplitudes between −0.5 to 0.5 V/Å for many of the atom cases we have tested. The magnitudes of these fields are experimentally achievable in graphene devices.[1] The slope of each line gives the strain piezoelectric coefficient, d_{31}, for each atom (see Supporting Information). The d_{31} coefficients for all cases are highlighted in Table 1. We observe that there are significant variations in piezoelectric properties with respect to the dopant, more than a factor of 3. Binding F to graphene results in a very small change to the piezoelectric coefficient.

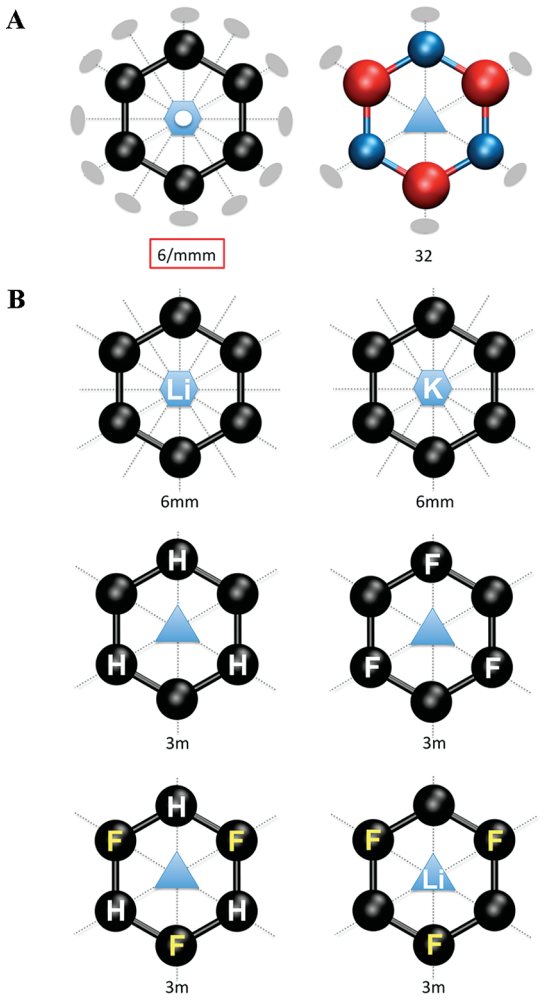

Figure 2. (A) Point group symmetry for graphene and hexagonal boron nitride (h-BN). Red box around point group label indicates inversion symmetry is present. h-BN lacks inversion symmetry, leading to piezoelectricity. (B) Point group symmetry of lattice unit cells for each case of atom adsorption considered here. We employ periodic boundary conditions. In all cases, inversion symmetry is destroyed, leading to piezoelectricity. A hexagon or triangle in the center represents a C_6 or C_3 rotational axes, respectively, while dotted lines indicate mirror plane symmetry. Gray ovals represent a 2-fold rotational (diad) axis and a white dot in the center indicates a rotoinversion symmetry. Carbon atoms are colored black, boron atoms are colored red, and nitrogen atoms are colored blue. White-labeled atoms indicate binding above the graphene sheet while yellow-labeled atoms indicate binding below the sheet. Hexagonal or trigonal point group symmetry results if an atom prefers to bind at the hollow site or top site.

A similar observation is made when binding H and F together on opposite sides of graphene. Both alkali metal atoms that we tested (Li and K) result in moderate changes in piezoelectricity. We find that adding F to the top site (over a carbon atom) and Li to the hollow site on the opposite side gives the largest value of d_{31}.

For context, we would like to compare our calculated values to values of known piezoelectric materials. We find that the maximum d_{31} coefficient that we calculated (3.0×10^{-1} pm/V) is comparable to a theoretical value of 3.3×10^{-1} pm/V for wurtzite boron nitride (BN)[55] and a factor of 3 lower than that of wurtzite GaN (−1.0 pm/V).[56] The latter are both 4-fold coordinated 3D materials with completely different structures than the 2D materials. Despite these differences, the piezo coefficients for doped graphene are comparable. Note that the sign of the d_{31} coefficient will depend on the choice of the 3-axis direction.

To determine the e_{31} piezo coefficients, we have calculated the polarization change perpendicular to the surface as a function of equibiaxial in-plane strain in Figure 3b. For low strains between −1% to 1%, we find that the relationship is linear for all atoms. The slope of each line gives twice the e_{31} piezoelectric coefficient for each atom due to the equibiaxial in-plane strain employed (see Supporting Information). Table 1 shows that both alkali metals have the highest piezoelectric coefficients, almost twice as much as the other cases tested. Unlike the d_{31} coefficients, we find that the addition of Li to F on graphene does not lead to a significant enhancement of the e_{31} coefficient.

To make a direct comparison to a 3D material like wurtzite BN or GaN, we must take into account the difference in dimensionality since the coefficient units for 2D materials are charge per unit length, while for 3D materials, they are charge per unit area. A rough account can be made for the dimensionality[34] by dividing the e_{31} coefficient of Li adsorbed on graphene by the graphite interlayer spacing of 3.35 Å,[57] providing a value of $e_{31,3D}$ of 0.17 C/m^2. We have also computed $e_{31,3D}$ using the elastic stiffness tensor of graphite[58] and our calculated $d_{31,}$ yielded a similar value of 0.19 C/m^2 (see Supporting Information). Comparing this to the calculated $e_{11,3D}$ of 0.731 C/m^2 for 2D h-BN,[59] it is smaller by more than a factor of 4. However, the e_{11} and e_{31} coefficients are not directly comparable since the e_{11} coefficient is generally larger. If we compare our calculated $e_{31,3D}$ to those of other bulk materials, we find it is within a factor of 2 of the theoretical value[55] of 0.31 C/m^2 obtained for wurtzite BN and approximately a factor of 3 less than the experimental value[60] of −0.55 C/m^2 for wurtzite GaN. It is notable here that the polarization magnitudes in the graphene case have the potential to be larger than those of wurtzite GaN due to the larger elastic strains achievable in graphene before elastic failure (critical strain larger than 10%).[24] Our results for both the stress and strain piezoelectric coefficients demonstrate that it is possible to engineer piezoelectricity into graphene that is comparable to known piezoelectric materials.

Since it might be expected that piezoelectric effects should be observable only for sufficiently large dopant concentrations, we have examined how the piezoelectric coefficients change as a function of atom coverage. Using lithium as an example, we modeled a range of atom coverage densities by putting a single Li atom on a 1 × 1, 2 × 2, 3 × 3, and 4 × 4 graphene

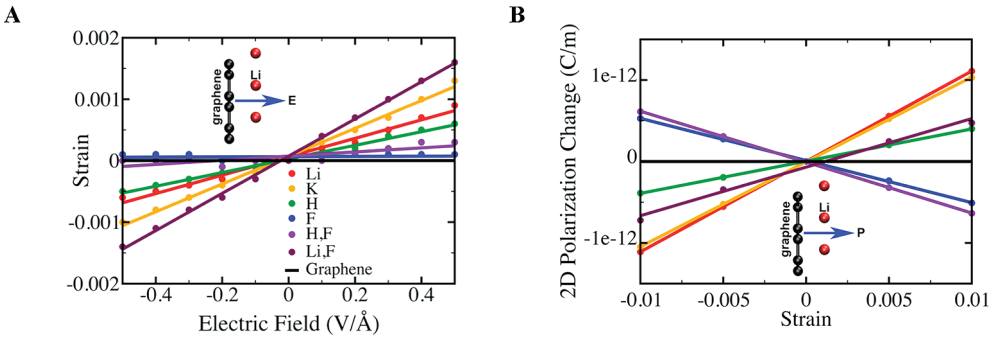

Figure 3. (A) An external electric field applied perpendicular to the graphene sheet induces an equibiaxial strain in the plane of the sheet. This results in a linear relationship between the electric field and strain at low fields, the slope of which gives the d_{31} piezoelectric coefficient. Shown are calculations for the atom dopants depicted in Figure 1. Inset indicates the direction of the positive electric field. (B) Applying an equibiaxial in-plane strain to graphene induces a change in the polarization perpendicular to the sheet. At low strains, this relationship is linear where the slope gives twice the e_{31} piezoelectric coefficient. Inset designates the direction of positive polarization.

TABLE 1. Values for the d_{31} and e_{31} Piezoelectric Coefficients for All Atom Cases[a]

atom(s)	d_{31} (pm/V)	e_{31} (C/m)
Li	1.5×10^{-1}	5.5×10^{-11}
K	2.3×10^{-1}	5.2×10^{-11}
H	1.1×10^{-1}	2.0×10^{-11}
F	1.8×10^{-3}	-2.6×10^{-11}
H,F	3.4×10^{-2}	-3.1×10^{-11}
F,Li	3.0×10^{-1}	3.0×10^{-11}

[a] Doping with both F and Li give the largest d_{31} piezoelectric coefficient while doping with either Li or K gives the largest e_{31} piezoelectric coefficient.

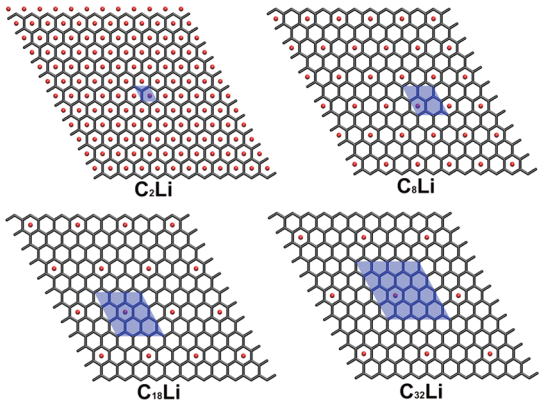

Figure 4. Different concentrations of Li on graphene. Unit cell is highlighted in blue and denoted by the formula unit C_nLi where $n = 2$, 8, 18, and 32. Periodic boundary conditions are employed in all cases.

periodic supercell. This is depicted in Figure 4 where the unit cells are highlighted in blue. These systems are labeled by the formula unit C_nLi where $n = 2$, 8, 18, and 32, respectively. Figure 5a shows the equibiaxial in-plane strain on the graphene sheet as a function of electric field. The relationship between the field and strain varies with the coverage of Li on the graphene surface. In the inset of Figure 5a, we plot the value of the d_{31} coefficient as a function of Li coverage. We find a maximum in the piezoelectric coefficient at C_8Li,

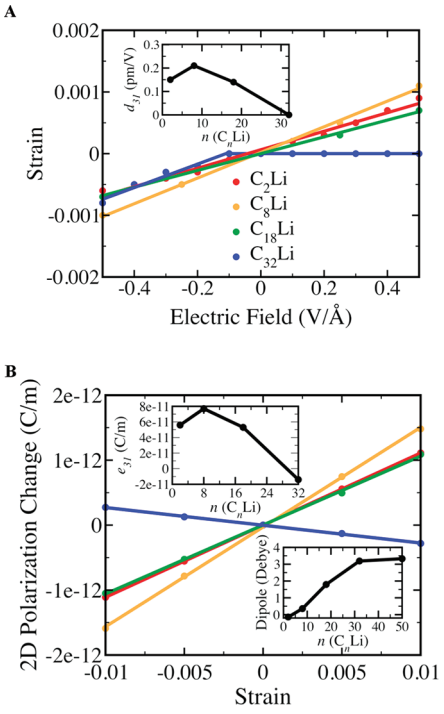

Figure 5. (A) Equibiaxial in-plane strain as a function of electric field applied perpendicular to the plane for different coverage densities of Li on graphene. The inset shows that a maximum in the d_{31} piezoelectric coefficient occurs for C_8Li or 1 Li for every eight carbon atoms. (B) Change in the polarization perpendicular to the plane as a function of equibiaxial in-plane strain for different coverage densities of Li on graphene. The top inset indicates that a maximum in the e_{31} piezoelectric coefficient occurs for C_8Li similar to that in panel A. The bottom inset indicates how the static dipole moment changes as a function of Li coverage. Convergence of the dipole moment is reached for the case of $C_{32}Li$ or one Li for every 32 carbon atoms.

which corresponds to one Li atom for every eight carbon atoms (2×2 supercell). As coverage decreases, we see that the piezoelectric coefficient becomes smaller and eventually reaches near-zero for $C_{32}Li$ or one Li atom for every 32 carbon atoms (4×4 supercell). We find that the static dipole moment of Li on graphene

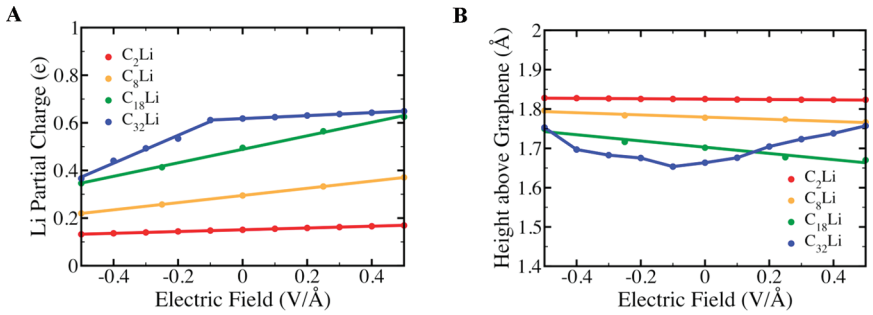

Figure 6. (A) Löwdin analysis for the partial charge on Li as a function of applied electric field at different concentrations on graphene. Linear relationship observed for all but $C_{32}Li$ case, similar to trends for d_{31}. Charge transfer occurs with a change in field for fields more negative than −0.1 V/Å. (B) Li height above graphene as a function of applied electric field for different Li coverages. For $C_{32}Li$, the minimum was observed at −0.1 V/Å. For fields more positive than −0.1 V/Å, the charge is fixed on Li while moving away from graphene. For fields more negative than −0.1 V/Å, charge transfer takes place as the Li height above graphene increases.

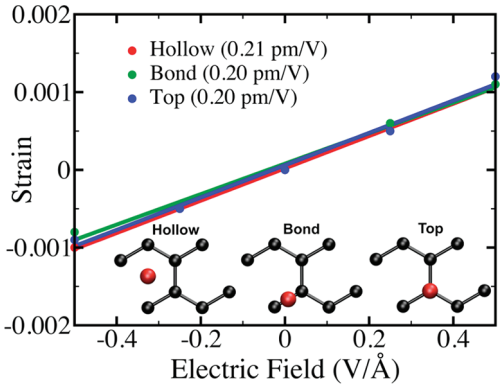

Figure 7. Equibiaxial in-plane strain as a function of applied electric field for different positions (hollow, bond and top site) of Li on graphene for C_8Li. Unit cells for each of these positions are given in the inset. In all cases, the calculated d_{31} coefficients given in the legend are similar demonstrating that the position does not strongly affect the piezoelectric coefficient.

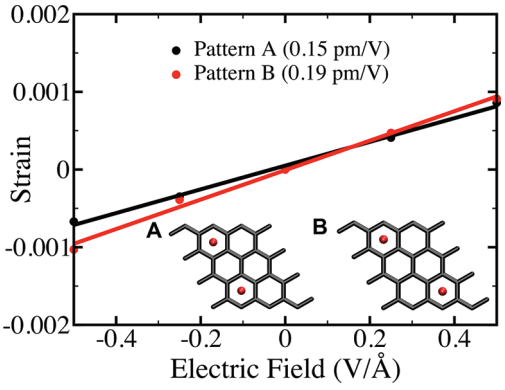

Figure 8. Equibiaxial in-plane strain as a function of applied electric field for two different crystal patterns of $C_{32}Li_2$. Unit cells for each of these patterns are given in the inset. Different arrangements of Li atoms on surface result in changes in the d_{31} piezoelectric coefficient by approximately 20%.

increases as the coverage decreases, leading to a stronger interaction with the field (Figure 5b bottom inset). However, the enhanced interaction is diminished by the ratio of Li to C atoms at low coverages. The competition between these effects provides a maximum in the Figure 5a inset.

The e_{31} coefficient follows a similar trend as the d_{31} as shown in Figure 5b. The top inset of Figure 5b shows that a maximum is again reached for C_8Li or one Li atom for every 8 carbon atoms. Low coverage again leads to small values, including a possible sign flip. The results we have obtained for both d_{31} and e_{31} as a function of coverage, therefore, show that the magnitude of piezoelectricity in graphene can be engineered by varying the concentration of atoms on the surface.

The case of $C_{32}Li$ exhibits nonlinear behavior (nonlinear piezoelectricity) in d_{31} for fields more negative than −0.1 V/Å. The d_{31} piezoelectric coefficient is approximately zero only for small field magnitudes. For fields more negative than −0.1 V/Å, there is an abrupt nonlinear behavior and onset of linear decrease in the strain with a slope of 0.19 pm/V, similar to higher coverage cases. We find that this nonlinearity is associated with the onset of a charge transfer process between Li and graphene that occurs at −0.1 V/Å fields. We have performed a Löwdin analysis to calculate the partial charges on Li, which are shown in Figure 6a as a function of applied field for each concentration studied. We see that for fields more positive than −0.1 V/Å, partial charge on Li remains constant, but for fields more negative than −0.1 V/Å, there is significant charge transfer. Furthermore, if we examine how the height of Li above graphene changes as a function of field for each coverage (Figure 6b), we find there is a minimum at −0.1 V/Å for $C_{32}Li$ compared to the other coverages, which are relatively linear. For fields more positive than −0.1 V/Å, the charge is fixed as the distance from Li to graphene increases. For applied fields more negative than −0.1 V/Å, charge transfer takes place while the Li moves away from graphene. These results suggest that the large piezoelectric response for applied fields more negative than −0.1 V/Å is associated with charge transfer from graphene to Li.

We have also examined the effect of adatom positions on the piezoelectric response. Potassium and lithium atoms are found to be relatively mobile on the surface of graphite and graphene.[41,49,50] Such diffusion of

atoms away from the configurations studied in Figure 1 is not expected to destroy the d_{31} and e_{31} piezoelectricity because centrosymmetry is absent regardless of the adatom location. Using a coverage of C_8Li, we have calculated d_{31} coefficients for cases where the Li atom is positioned either at the hollow, bond, or top site. In Figure 7, we show how equibiaxial in-plane strain varies under applied electric fields perpendicular to the surface for these adatom positions. We find that the slopes, and hence the d_{31} coefficients, are within 5% of each other. These results indicate that the piezoelectric response does not strongly depend on adatom location.

In addition to adatom position, we have studied the effect of crystallographic patterning of adatoms on the graphene surface for a fixed concentration of $C_{32}Li_2$. Two lithium atoms are placed in different hollow sites as shown in the inset of Figure 8. Our results show that there is an approximately 20% change in the d_{31} piezoelectric coefficient depending on how the Li atoms are positioned with respect to each other. The coefficients are similar to the $C_{18}Li$ case which has similar stoichiometry. Patterning appears unlikely to result in substantive changes to the piezoelectric coefficients we have calculated in this work.

While we have focused these studies on adsorbed atoms, one might imagine that in-plane defects of graphene like vacancies or substitutional impurities may generate a piezoelectric effect. However, we expect in-plane defects to exhibit inversion symmetry to a significant degree, and therefore, lack a significant piezoelectric effect.

CONCLUSION

Engineered piezoelectricity at the nanoscale may lead to new devices, from electronics and photonics to energy harvesting, chemical sensing, and high frequency acoustics. Adsorbing atoms on the surface of graphene breaks inversion symmetry, inducing piezoelectricity of magnitudes comparable to known values for other 2D and 3D materials. Unlike existing piezoelectric materials, this fundamentally new form of piezoelectricity is *engineered* into a nonpiezoelectric material, made possible by the 2D nanoscale nature of graphene. The applied electric fields[1] and chemical doping[40,41] required to observe these effects in graphene are readily experimentally accessible. For example, chemically stable, single-sided hydrogen and fluorine adatom deposition has already been demonstrated.[35−37] We see that doping with a combination of F and Li results in the largest change in the d_{31} piezoelectric coefficient while doping with only Li results in the greatest change in the e_{31} coefficient. Our study of Li surface coverage shows that the piezoelectric coefficients reach a nontrivial maximum when there is one Li atom for every 8 carbon atoms. A coverage of $C_{32}Li$ exhibits nonlinear behavior in d_{31} at fields of -0.1 V/Å, which can be attributed to abrupt charge transfer from graphene to Li. Furthermore, we have seen that positioning and patterning of Li on graphene do not result in significant changes to the piezoelectric coefficient. The demonstrated experimental ability to spatially pattern adsorbates on the graphene surface[37−39] could lead to devices where, for example, strains are spatially concentrated to control local electrical and chemical properties. We envision that this work could potentially lead to the creation of new piezoelectric devices based not just on graphene, but other 2D and low-dimensional materials as well.

METHODS

We use density functional theory implemented within the Quantum-ESPRESSO *ab initio* software package.[51] Ion cores are treated using ultrasoft (Vanderbilt) pseudopotentials[61] in all cases except for potassium, which was treated using a norm-conserving pseudopotential.[62] A nonlinear core correction is included for both potassium and fluorine. Electron exchange and correlation effects are described using the spin-polarized generalized-gradient corrected Perdew−Burke−Ernzerhof (PBE) approximation.[52] All calculations were done using periodic boundary conditions and a primitive cell with one atom for every two carbon atoms except when noted. The electronic wave function is expanded in a plane wave basis set with an energy cutoff of 60 Ry. Brillouin zone sampling was done using a Monkhorst-Pack mesh[63] of $14 \times 14 \times 1$ for all atom cases and a Gaussian smearing of 0.02 eV was used for the electronic occupations. We scaled this k-point mesh to $8 \times 8 \times 1$, $6 \times 6 \times 1$, and $4 \times 4 \times 1$ for a 2×2, 3×3, and 4×4 supercell, respectively, in order to study atom surface coverage effects. A 20 Å computational lattice cell dimension in the *z*-direction (perpendicular to the graphene sheet) was used to prevent periodic images of graphene from interacting with each other. All ionic relaxations and cell optimization were performed using a force convergence threshold of 3×10^{-4} Ry/au. Single atom adsorption on one side gives rise to an asymmetric surface with a net electric dipole moment. We use a dipole correction to cancel out the artificial electrical field that arises from this dipole moment.[64]

Acknowledgment. Our work was performed at Stanford University and supported in part by the U.S. Army Research Laboratory, through the Army High Performance Computing Research Center, Cooperative Agreement W911NF-07-0027. This research also used resources of the National Energy Research Scientific Computing Center (NERSC), which is supported by the Office of Science of the U.S. Department of Energy under Contract No. DE-AC02-05CH11231. Some calculations were performed in part using the Stanford NNIN Computing Facility (SNCF), a member of the National Nanotechnology Infrastructure Network (NNIN), supported by the National Science Foundation (NSF). The authors would also like to thank Dr. Tingting Qi, Lenson Pellouchoud, and Karel-Alexander Duerloo for useful comments and discussion about this manuscript.

Supporting Information Available: Additional details about the piezoelectric tensor and its relationship to symmetry, how the piezoelectric coefficients e_{31} and d_{31} are calculated, how e_{31} and d_{31} relate to each other, and a comparison of in-plane strain from atom adsorption on the surface and additional strain from application of an electric field. This material is available free of charge *via* the Internet at http://pubs.acs.org.

REFERENCES AND NOTES

1. Zhang, Y.; Tang, T.-T.; Girit, C.; Zhao, H.; Martin, M. C.; Zettl, A.; Crommie, M. F.; Shen, Y. R.; Feng, W. Direct Observation of a Widely Tunable Bandgap in Bilayer Graphene. *Nature* **2009**, *459*, 820–823.
2. Wang, Z. L.; Song, J. H. Piezoelectric Nanogenerators Based on Zinc Oxide Nanowire Arrays. *Science* **2006**, *312*, 242–246.
3. Oostinga, J. B.; Heersche, H. B.; Liu, X. L.; Morpurgo, A. F.; Vandersypen, L. M. K. Gate-Induced Insulating State in Bilayer Graphene Devices. *Nat. Mater.* **2008**, *7*, 151–157.
4. Bunch, J. S.; Verbridge, S. S.; Alden, J. S.; van der Zande, A. M.; Parpia, J. M.; Craighead, H. G.; McEuen, P. L. Impermeable Atomic Membranes from Graphene Sheets. *Nano Lett.* **2008**, *8*, 2458–2462.
5. Craighead, H. G. Nanoelectromechanical Systems. *Science* **2000**, *290*, 1532–1535.
6. Fennimore, A. M.; Yuzvinsky, T. D.; Han, W. Q.; Fuhrer, M. S.; Cumings, J.; Zettl, A. Rotational Actuators Based on Carbon Nanotubes. *Nature* **2003**, *424*, 408–410.
7. Park, S.; An, J.; Suk, J. W.; Ruoff, R. S. Graphene-Based Actuators. *Small* **2010**, *6*, 210–212.
8. van Delden, R. A.; ter Wiel, M. K. J.; Pollard, M. M.; Vicario, J.; Koumura, N.; Feringa, B. L. Unidirectional Molecular Motor on a Gold Surface. *Nature* **2005**, *437*, 1337–1340.
9. Requicha, A. A. G. Nanorobots, NEMS, and Nanoassembly. *Proc. IEEE* **2003**, *91*, 1922–1933.
10. Shirai, Y.; Osgood, A. J.; Zhao, Y. M.; Kelly, K. F.; Tour, J. M. Directional Control in Thermally Driven Single-Molecule Nanocars. *Nano Lett.* **2005**, *5*, 2330–2334.
11. Novoselov, K. S.; Geim, A. K.; Morozov, S. V.; Jiang, D.; Zhang, Y.; Dubonos, S. V.; Grigorieva, I. V.; Firsov, A. A. Electric Field Effect in Atomically Thin Carbon Films. *Science* **2004**, *306*, 666–669.
12. Levy, N.; Burke, S. A.; Meaker, K. L.; Panlasigui, M.; Zettl, A.; Guinea, F.; Neto, A. H. C.; Crommie, M. F. Strain-Induced Pseudo-magnetic Fields Greater Than 300 T in Graphene Nanobubbles. *Science* **2010**, *329*, 544–547.
13. Bao, W. Z.; Miao, F.; Chen, Z.; Zhang, H.; Jang, W. Y.; Dames, C.; Lau, C. N. Controlled Ripple Texturing of Suspended Graphene and Ultrathin Graphite Membranes. *Nat. Nanotechnol.* **2009**, *4*, 562–566.
14. Fogler, M. M.; Castro Neto, A. H.; Guinea, F. Effect of External Conditions on the Structure of Scrolled Graphene Edges. *Phys. Rev. B* **2010**, *81*, 161408.
15. Fogler, M. M.; Guinea, F.; Katsnelson, M. I. Pseudomagnetic Fields and Ballistic Transport in a Suspended Graphene Sheet. *Phys. Rev. Lett.* **2008**, *101*, 226804.
16. Fujita, T.; Jalil, M. B. A.; Tan, S. G. Valley Filter in Strain Engineered Graphene. *Appl. Phys. Lett.* **2010**, *97*, 043508.
17. Guinea, F.; Katsnelson, M. I.; Geim, A. K. Energy Gaps and a Zero-Field Quantum Hall Effect in Graphene by Strain Engineering. *Nat. Phys.* **2010**, *6*, 30–33.
18. Hossain, M. Z. Quantum Conductance Modulation in Graphene by Strain Engineering. *Appl. Phys. Lett.* **2010**, *96*, 143118.
19. Pereira, V. M.; Neto, A. H. C. Strain Engineering of Graphene's Electronic Structure. *Phys. Rev. Lett.* **2009**, *103*, 046801.
20. Morten, B.; Decicco, G.; Prudenziati, M. Resonant Pressure Sensor Based on Piezoelectric Properties of Ferroelectric Thick-Films. *Sens. Actuator A-Phys.* **1992**, *31*, 153–158.
21. Jaffe, H.; Berlincourt, D. A. Piezoelectric Transducer Materials. *Proc. IEEE* **1965**, *53*, 1372–1386.
22. Agrawal, R.; Espinosa, H. D. Giant Piezoelectric Size Effects in Zinc Oxide and Gallium Nitride Nanowires. A First Principles Investigation. *Nano Lett.* **2011**, *11*, 786–790.
23. Sharma, N. D.; Maranganti, R.; Sharma, P. On the Possibility of Piezoelectric Nanocomposites without Using Piezoelectric Materials. *J. Mech. Phys. Solids* **2007**, *55*, 2328–2350.
24. Lee, C.; Wei, X. D.; Kysar, J. W.; Hone, J. Measurement of the Elastic Properties and Intrinsic Strength of Monolayer Graphene. *Science* **2008**, *321*, 385–388.
25. Ferralis, N.; Maboudian, R.; Carraro, C. Evidence of Structural Strain in Epitaxial Graphene Layers on 6*H*-SiC(0001). *Phys. Rev. Lett.* **2008**, *101*, 156801.
26. Teague, M. L.; Lai, A. P.; Velasco, J.; Hughes, C. R.; Beyer, A. D.; Bockrath, M. W.; Lau, C. N.; Yeh, N. C. Evidence for Strain-Induced Local Conductance Modulations in Single-Layer Graphene on SiO_2. *Nano Lett.* **2009**, *9*, 2542–2546.
27. Kim, K. S.; Zhao, Y.; Jang, H.; Lee, S. Y.; Kim, J. M.; Kim, K. S.; Ahn, J.-H.; Kim, P.; Choi, J.-Y.; Hong, B. H. Large-Scale Pattern Growth of Graphene Films for Stretchable Transparent Electrodes. *Nature* **2009**, *457*, 706–710.
28. Pereira, V. M.; Neto, A. H. C.; Peres, N. M. R. Tight-binding Approach to Uniaxial Strain in Graphene. *Phys. Rev. B* **2009**, *80*, 045401.
29. Mohiuddin, T. M. G.; Lombardo, A.; Nair, R. R.; Bonetti, A.; Savini, G.; Jalil, R.; Bonini, N.; Basko, D. M.; Galiotis, C.; Marzari, N.; *et al*. Uniaxial Strain in Graphene by Raman Spectroscopy: G Peak Splitting, Gruneisen Parameters, and Sample Orientation. *Phys. Rev. B* **2009**, *79*, 205433.
30. Yu, T.; Ni, Z.; Du, C.; You, Y.; Wang, Y.; Shen, Z. Raman Mapping Investigation of Graphene on Transparent Flexible Substrate: The Strain Effect. *J. Phys. Chem. B* **2008**, *112*, 12602–12605.
31. Nye, J. F. *Physical Properties of Crystals: Their Representation by Tensors and Matrices*; Clarendon Press: Oxford, 1957.
32. Michel, K. H.; Verberck, B. Theory of Elastic and Piezoelectric Effects in Two-Dimensional Hexagonal Boron Nitride. *Phys. Rev. B* **2009**, *80*, 224301.
33. Naumov, I.; Bratkovsky, A. M.; Ranjan, V. Unusual Flexoelectric Effect in Two-Dimensional Noncentrosymmetric sp(2)-Bonded Crystals. *Phys. Rev. Lett.* **2009**, *102*, 217601.
34. Sai, N.; Mele, E. J. Microscopic Theory for Nanotube Piezoelectricity. *Phys. Rev. B* **2003**, *68*, 241405.
35. Elias, D. C.; Nair, R. R.; Mohiuddin, T. M. G.; Morozov, S. V.; Blake, P.; Halsall, M. P.; Ferrari, A. C.; Boukhvalov, D. W.; Katsnelson, M. I.; Geim, A. K.; *et al*. Control of Graphene's Properties by Reversible Hydrogenation: Evidence for Graphane. *Science* **2009**, *323*, 610–613.
36. Nair, R. R.; Ren, W. C.; Jalil, R.; Riaz, I.; Kravets, V. G.; Britnell, L.; Blake, P.; Schedin, F.; Mayorov, A. S.; Yuan, S. J.; *et al*. Fluorographene: A Two-Dimensional Counterpart of Teflon. *Small* **2010**, *6*, 2877–2884.
37. Robinson, J. T.; Burgess, J. S.; Junkermeier, C. E.; Badescu, S. C.; Reinecke, T. L.; Perkins, F. K.; Zalalutdniov, M. K.; Baldwin, J. W.; Culbertson, J. C.; Sheehan, P. E.; *et al*. Properties of Fluorinated Graphene Films. *Nano Lett.* **2010**, *10*, 3001–3005.
38. Sessi, P.; Guest, J. R.; Bode, M.; Guisinger, N. P. Patterning Graphene at the Nanometer Scale *via* Hydrogen Desorption. *Nano Lett.* **2009**, *9*, 4343–4347.
39. Balog, R.; Jorgensen, B.; Nilsson, L.; Andersen, M.; Rienks, E.; Bianchi, M.; Fanetti, M.; Laegsgaard, E.; Baraldi, A.; Lizzit, S.; *et al*. Bandgap Opening in Graphene Induced by Patterned Hydrogen Adsorption. *Nat. Mater.* **2010**, *9*, 315–319.
40. Chen, J. H.; Jang, C.; Adam, S.; Fuhrer, M. S.; Williams, E. D.; Ishigami, M. Charged-Impurity Scattering in Graphene. *Nat. Phys.* **2008**, *4*, 377–381.
41. Ohta, T.; Bostwick, A.; Seyller, T.; Horn, K.; Rotenberg, E. Controlling the Electronic Structure of Bilayer Graphene. *Science* **2006**, *313*, 951–954.
42. Chan, K. T.; Neaton, J. B.; Cohen, M. L. First-Principles Study of Metal Adatom Adsorption on Graphene. *Phys. Rev. B* **2008**, *77*, 235430.
43. Jin, K. H.; Choi, S. M.; Jhi, S. H. Crossover in the Adsorption Properties of Alkali Metals on Graphene. *Phys. Rev. B* **2010**, *82*, 033414.
44. Klintenberg, M.; Lebegue, S.; Katsnelson, M. I.; Eriksson, O. Theoretical Analysis of the Chemical Bonding and Electronic Structure of Graphene Interacting with Group IA and Group VIIA Elements. *Phys. Rev. B* **2010**, *81*, 085433.
45. Lugo-Solis, A.; Vasiliev, I. *Ab Initio* Study of K Adsorption on Graphene and Carbon Nanotubes: Role of Long-Range Ionic Forces. *Phys. Rev. B* **2007**, *76*, 235431.
46. Bennich, P.; Puglia, C.; Bruhwiler, P. A.; Nilsson, A.; Maxwell, A. J.; Sandell, A.; Martensson, N.; Rudolf, P. Photoemission Study of K on Graphite. *Phys. Rev. B* **1999**, *59*, 8292–8304.

47. Caragiu, M.; Finberg, S. Alkali Metal Adsorption on Graphite: A Review. *J. Phys.-Condens. Matter* **2005**, *17*, R995–R1024.
48. Hu, Z. P.; Ignatiev, A. Lithium Adsorption on the Graphite (0001) Surface. *Phys. Rev. B* **1984**, *30*, 4856–4859.
49. Osterlund, L.; Chakarov, D. V.; Kasemo, B. Potassium Adsorption on Graphite(0001). *Surf. Sci.* **1999**, *420*, 174–189.
50. Virojanadara, C.; Watcharinyanon, S.; Zakharov, A. A.; Johansson, L. I. Epitaxial Graphene on 6H-SiC and Li Intercalation. *Phys. Rev. B* **2010**, *82*, 205402.
51. Giannozzi, P.; Baroni, S.; Bonini, N.; Calandra, M.; Car, R.; Cavazzoni, C.; Ceresoli, D.; Chiarotti, G. L.; Cococcioni, M.; Dabo, I., *et al*., Quantum Espresso: A Modular and Open-source Software Project for Quantum Simulations of Materials. *J. Phys.-Condens. Matter* **2009**, *21*, 395502.
52. Perdew, J. P.; Burke, K.; Ernzerhof, M. Generalized Gradient Approximation Made Simple. *Phys. Rev. Lett.* **1996**, *77*, 3865–3868.
53. Sofo, J. O.; Chaudhari, A. S.; Barber, G. D. Graphane: A Two-Dimensional Hydrocarbon. *Phys. Rev. B* **2007**, *75*, 153401.
54. Kunc, K.; Resta, R. External Fields in the Self-Consistent Theory of Electronic States: A New Method for Direct Evaluation of Macroscopic and Microscopic Dielectric Response. *Phys. Rev. Lett.* **1983**, *51*, 686–689.
55. Shimada, K. First-Principles Determination of Piezoelectric Stress and Strain Constants of Wurtzite III-V Nitrides. *Jpn. J. Appl. Phys.* **2006**, *45*, L358–L360.
56. Hangleiter, A.; Hitzel, F.; Lahmann, S.; Rossow, U. Composition Dependence of Polarization Fields in GaInN/GaN Quantum Wells. *Appl. Phys. Lett.* **2003**, *83*, 1169–1171.
57. Bacon, G. E. The Interlayer Spacing of Graphite. *Acta Crystallogr.* **1951**, *4*, 558–561.
58. Blakslee, O. L.; Proctor, D. G.; Seldin, E. J.; Spence, G. B.; Weng, T. Elastic Constants of Compression-Annealed Pyrolytic Graphite. *J. Appl. Phys.* **1970**, *41*, 3373–3382.
59. Michel, K. H.; Verberck, B. Phonon Dispersions and Piezoelectricity in Bulk and Multilayers of Hexagonal Boron Nitride. *Phys. Rev. B* **2011**, *83*, 115328.
60. Guy, I. L.; Muensit, S.; Goldys, E. M. Extensional Piezoelectric Coefficients of Gallium Nitride and Aluminum Nitride. *Appl. Phys. Lett.* **1999**, *75*, 4133–4135.
61. Vanderbilt, D. Soft Self-Consistent Pseudopotentials in a Generalized Eigenvalue Formalism. *Phys. Rev. B* **1990**, *41*, 7892–7895.
62. Bachelet, G. B.; Schluter, M. Relativistic Norm-conserving Pseudopotentials. *Phys. Rev. B* **1982**, *25*, 2103–2108.
63. Monkhorst, H. J.; Pack, J. D. Special Points for Brillouin-Zone Integrations. *Phys. Rev. B* **1976**, *13*, 5188–5192.
64. Bengtsson, L. Dipole Correction for Surface Supercell Calculations. *Phys. Rev. B* **1999**, *59*, 12301–12304.